



Utilizing Intraoperative Navigated 3D Color Doppler Ultrasound in Glioma Surgery

Benjamin Saß^{1*}, Mirza Pojskic¹, Darko Zivkovic¹, Barbara Carl^{1,2}, Christopher Nimsky^{1,3} and Miriam H. A. Bopp^{1,3}

¹ Department of Neurosurgery, University of Marburg, Marburg, Germany, ² Department of Neurosurgery, Helios Dr. Horst Schmidt Kliniken, Wiesbaden, Germany, ³ Center for Mind, Brain and Behavior (CMBB), Marburg, Germany

OPEN ACCESS

Edited by:

Francesco DiMeo,
Fondazione IRCCS Istituto
Neurologico Carlo Besta, Italy

Reviewed by:

Massimiliano Del Bene,
Dipartimento di Neurochirurgia, Istituto
Neurologico Carlo Besta (IRCCS), Italy

Andrej Steno,
Comenius University, Slovakia

*Correspondence:

Benjamin Saß
sassb@med.uni-marburg.de

Specialty section:

This article was submitted to
Neuro-Oncology and
Neurosurgical Oncology,
a section of the journal
Frontiers in Oncology

Received: 20 January 2021

Accepted: 23 July 2021

Published: 18 August 2021

Citation:

Saß B, Pojskic M, Zivkovic D, Carl B,
Nimsky C and Bopp MHA (2021) Utilizing
Intraoperative Navigated 3D Color
Doppler Ultrasound in Glioma Surgery.
Front. Oncol. 11:656020.
doi: 10.3389/fonc.2021.656020

Background: In glioma surgery, the patient's outcome is dramatically influenced by the extent of resection and residual tumor volume. To facilitate safe resection, neuronavigational systems are routinely used. However, due to brain shift, accuracy decreases with the course of the surgery. Intraoperative ultrasound has proved to provide excellent live imaging, which may be integrated into the navigational procedure. Here we describe the visualization of vascular landmarks and their shift during tumor resection using intraoperative navigated 3D color Doppler ultrasound (3D iUS color Doppler).

Methods: Six patients suffering from glial tumors located in the temporal lobe were included in this study. Intraoperative computed tomography was used for registration. Datasets of 3D iUS color Doppler were generated before dural opening and after tumor resection, and the vascular tree was segmented manually. In each dataset, one to four landmarks were identified, compared to the preoperative MRI, and the Euclidean distance was calculated.

Results: Pre-resectional mean Euclidean distance of the marked points was 4.1 ± 1.3 mm (mean \pm SD), ranging from 2.6 to 6.0 mm. Post-resectional mean Euclidean distance was 4.7 ± 1.0 mm, ranging from 2.9 to 6.0 mm.

Conclusion: 3D iUS color Doppler allows estimation of brain shift intraoperatively, thus increasing patient safety. Future implementation of the reconstructed vessel tree into the navigational setup might allow navigational updating with further consecutive increase of accuracy.

Keywords: intraoperative ultras, color Doppler ultrasound, intraoperative imaging, brain shift, glioma

INTRODUCTION

Gliomas are the most common primary brain tumors representing 27% of all brain and central nervous system (CNS) tumors and 80% of malignant brain tumors in the United States (US) population (1). The broad category of gliomas encompasses tumors of astrocytic, oligodendrocytic, or ependymal origin and is classified by the World Health Organization (WHO) into four grades, depending on histological and molecular characteristics (2). Grade I tumors, typically

seen in children, are potentially curable when resected, whereas low-grade gliomas (WHO grade II), which are mostly seen in young adults, progress eventually to high-grade gliomas (3). The majority of gliomas (55.1%) are glioblastomas WHO grade IV, which occur with an incidence of 3.4 per 100,000 (1). The main cornerstones of glioma therapy include surgery for histological diagnosis and tumor removal, radiotherapy, and pharmacotherapy (4). There is an ongoing debate on the appropriate resection strategy, mainly driven by the demonstration of glioma cells within regions appearing to be normal brain tissue on cerebral magnetic resonance tomography (MRI) (5) and computed tomography (CT) (6, 7) and even in histologically normal brain regions (8). Several studies have proved the extent of resection (EOR) and the residual tumor volume in glioma surgery to be important factors influencing the patient's outcome as measured in progression-free survival and overall survival (9–12). Thus, it is common practice to resect as much tumor as possible while preserving neurological functions (13).

Prerequisite for this is the localization of pathological tissue as well as eloquent brain areas during the neurosurgical procedure, which can be realized using neuronavigational systems. These systems commonly utilize preoperative imaging, to which the patient is registered (14). Intraoperative imaging modalities such as computed tomography (iCT) (15–17), magnetic resonance tomography (iMRI) (18–20), and ultrasound (iUS) (21–23) can be integrated into these systems, improving safety and accuracy. Besides the possibility of instant resection control, intraoperative imaging can help the neurosurgeon to deal with brain shift, a well-described phenomenon, which is mostly due to brain swelling, loss of cerebrospinal fluid, tumor reduction, brain retraction, and influences of gravity after craniotomy and dural opening (24, 25). First efforts to estimate the extent of brain deformation date back to the 1980s (26). Since then various attempts have been made to approach this issue including optical scanning (27) and navigated pointer based surface displacement measurements (28, 29), a stereotactic system with integrated operative microscope and video analysis (24), iMRI (30, 31), and iUS (32–34). Brain shift has been shown to occur during the whole operative procedure, which can be partially addressed by serial MRI acquisitions as demonstrated by Nabavi et al. (35). The main limitations of iMRI are its restricted availability, structural requirements, time consumption, and high costs (36, 37). None of these drawbacks apply for iUS, which can be performed without significant interruption of the surgical procedure, is nowadays widely available, straightforward in use, and cost-effective (38). Modern ultrasound systems can be fully integrated into neuronavigational setups (39, 40) and are able to provide the neurosurgeon with information about resection extent in glioma surgery (40, 41) and brain deformation (39).

First descriptions of brain shift measurements utilizing iUS were published in the late 1990s, when specific, easily identifiable structures like the ventricles were marked in preoperative and intraoperative imaging to evaluate brain shifting (32–34). In 2003 Keles et al. analyzed pre- and postresectional navigated iUS

for brain shift correction and determination of resection extent (42). By that time iUS image quality and integration into navigational setups were rather poor, but improved successively the following years (39, 40, 43). In 2010 Ohue et al. described a new US-linked navigation system with improved imaging quality, which they used to quantify brain deformation at different anatomical (ventricles, meninges, sulci) or pathological structures (tumor boundaries) before and after dural opening and after tumor resection (22). These structures were identified in intraoperative brightness modulation (B-mode) ultrasound, whereas vessels can be visualized better in color or power Doppler mode. Already in 2001, Slomka et al. described a voxel-based registration of 3D Doppler ultrasound and preoperative MRI datasets using an iterative algorithm searching for the best geometric match in six cases (44). Rasmussen et al. examined postoperative automatic fusion of magnetic resonance angiogram (MRA) and intraoperative 3D Doppler ultrasound (i3D US Doppler) in five cases and found satisfactory results in terms of accuracy and time expenditure (45). In 2007 Reinertsen et al. intensified research in this respect and validated retrospectively an algorithm in five patients that used vascular centerlines extracted from both modalities to eventually achieve non-linear registration (46). The aforementioned investigations were feasibility studies outside the operating theater, and it took until 2014 to implement intraoperative use, when Reinertsen et al. reported an ultrasound-based registration method to correct for brain shift running during surgery. They performed semi-automatic registration based on MRA and i3D US Doppler datasets, in which the vascular tree was segmented, in seven cases (three vascular and four tumor procedures) and reported their method to be fully integrated into the neuronavigational system and ready to use (37). I3D US Doppler can also be sufficiently co-registered to other vascular imaging modalities, such as 3D digital subtraction angiography (DSA), as shown in 37 vascular cases by Podlesek et al., who utilized a curved linear array transducer capable of generating 3D volumes, which is typically used for endocavitary examinations in obstetrical, gynecological, and urological applications. They described iUS to be a valuable adjunct to established intraoperative vascular imaging modalities like indocyanine green angiography (ICG), although they did not integrate iUS into the navigational setup (47). Mohammadi et al. proposed and tested in a phantom and animal model a new approach for brain shift estimation utilizing a combination of surface imaging (stereo vision) and iUS Doppler, which were both registered to preoperative MRI respectively MRA datasets (48, 49). However, this approach has so far not entered clinical practice.

In our institution, i3D US datasets are routinely acquired during brain tumor resections, adding intraoperative live imaging to our multimodal neuronavigational setup. We have shown for brain metastasis that i3D US clearly delineates tumor boundaries and thereby allows pathologically based estimation of brain shift (50). Whilst tumor contours clearly identifiable with i3D US allow object analyzation and consecutive brain shift estimation in metastasis surgery, this becomes more challenging

in glioma surgery, where tumor boundaries are often not well defined in iUS. In the presented prospective work, we focused on brain shift estimation in glioma surgery utilizing preoperative MRI (preMRI) and i3D US Doppler datasets for the visualization of vascular structures. We designed this work as a proof-of-concept study to examine how the analysis of the vascular shift can be implemented in the preexisting navigational setup with as little workaround as possible to make it easily applicable for intraoperative use.

MATERIALS AND METHODS

To allow good visualization of vessels in i3D US, we only included patients suffering from gliomas and one case of a dysembroplastic neuroepithelial tumor (DNET), which were operated utilizing a temporal craniotomy. For more details see **Table 1**. Informed consent was obtained from all patients. Ethics approval was granted for prospective archiving clinical and technical data applying intraoperative imaging and navigation (study no. 99/18).

All patients underwent MRI imaging within a few days before surgery, typically including contrast-enhanced imaging and time-of-flight (ToF) sequences for vascular imaging. Preoperative imaging was transferred to the navigational system (Brainlab, Munich, Germany), consisting of a ceiling-mounted double monitor (Curve, Brainlab, Munich, Germany), a wall-mounted double display (Buzz, Brainlab, Munich, Germany), and navigational software.

All procedures were conducted under general anesthesia, and all patients received 40 mg of dexamethasone. After narcosis induction, the patients were positioned, the head placed horizontally and fixed to the OR (operating room) table using a radiolucent Doro head clamp with metallic pins. The pins were placed in such a way that in between intraoperative computed tomography (iCT) scanning for registration was possible without significant artifacts. A reference array with four reflective markers was attached to the head clamp. Although not necessary for registration, three fiducial markers were placed on the patient's head within the scanning range allowing registration accuracy measurements. After a 90° rotation of the OR table to the 32-slice mobile CT scanner (AIRO, Brainlab, Munich), a low-dose registration scan (0.042 mSv) of 62 mm scan length was performed. During the scanning process the navigational camera detected reflected markers permanently attached to the AIRO-scanner and the reference array. The

dataset was automatically transferred to the navigational system and fused to the preoperative imaging data to establish patient registration. After rotating the OR table back, the registration accuracy was checked by placing the tip of the navigational pointer in the divot of each of the three fiducial markers, which allowed calculation of the target registration error (TRE) as the Euclidean offset of the pointer tip. The reference array was removed and replaced by a sterile one after surgical skin preparation and sterile draping. Further details on the setup using iCT as an registration device were published before (51).

After team time-out, the skin was incised, and the temporalis muscle dissected. Subsequently, 125 ml of 15% mannitol were administered, and a temporal craniotomy performed. First sets of i3D US and i3D US Doppler data were acquired before dural opening using the ultrasound device bk5000 (bk medical, Herlev, Denmark) with a high resolution, small footprint transducer (N13C5, bk medical, Herlev, Denmark), which has a convex contact surface of 29 × 10 mm, a frequency range of 5–13 MHz, and is fully immersible and sterilizable. The pre-calibrated US probe was equipped with a reference array with three reflective markers. Saline was used as a coupling fluid, and the probe was swept gently over the dural layer for image acquisition. The generated 0.3 mm 2D slices were automatically transferred to the navigational system and transformed to co-registered 3D datasets. During the further surgical procedure, the i3D US and i3D US Doppler datasets were displayed either in an overlay view, side-by-side, or as standalone. After tumor resection, another set of US Doppler images was acquired in the same way in six cases.

For analysis of the vascular displacement, the vascular tree was segmented manually using a threshold-based filtering approach or outlined manually in ToF or T1 contrast-enhanced sequences. Because currently, the software does not allow threshold-based segmentation in i3D US Doppler datasets, in ultrasound images the vascular structures were segmented manually with the smart brush application (Brainlab navigational software, Munich, Germany), which is a computer-assisted outlining tool, allowing accelerated object segmentation. Representative, easily identifiable structures, such as vascular bifurcations, were marked in each dataset. To gain information on the brain deformation before dural opening, the Euclidean distance of the defined landmarks in preoperative MRI (preMRI) and pre-resectional i3D US Doppler was calculated. The brain shift occurring during the operative course was determined using the distance of the

TABLE 1 | Patient characteristics and tumor volume.

Case	Age [Years]	Diagnosis	Tumor volume [cm ³]
1	62.4	GBM	47.8
2	37.0	DA	71.5
3	40.8	GBM	39.9
4	71.4	DA*	67.5
5	35.2	DNET	20.4
6	55.6	GBM	41.3

GBM, glioblastoma; DA, diffuse astrocytoma; DA*, DA with molecular features of a glioblastoma WHO grade IV; DNET, dysembroplastic neuroepithelial tumor.

corresponding structures in post-resectional i3D US Doppler compared to preMRI.

GraphPad Prism 8.4.3 (GraphPad Software, San Diego, USA) for MacOS was used for statistical analysis. Under the assumption of normally distributed data, a paired t-test was used for further analysis. A p-value <0.05 was considered statistically significant.

RESULTS AND DISCUSSION

Six patients with temporal glial tumors were included in this study. The mean \pm standard deviation (SD) patient age was 50.4 ± 14.9 years, ranging from 35.2 to 71.4 years. The mean \pm SD tumor volume was 48.07 ± 19.00 cm³ (range: 20.4 to 71.5 cm³). Histopathological workup revealed glioblastoma in three cases. One case was classified as a diffuse astrocytary glioma with molecular features of a glioblastoma WHO grade IV, and one patient was diagnosed with WHO grade II diffuse astrocytoma. We also included one patient with a temporal DNET. The mean TRE was 0.82 ± 0.11 mm (mean \pm SD), depicting an excellent registration accuracy. Patient characteristics and tumor volume are summarized in **Table 1**.

The generation of 3D iUS Doppler image sets was straightforward. Pre-resectional 3D iUS Doppler was performed in all cases before dural opening. In case no. 3, the 3D iUS Doppler image set was corrupted by artifacts, primarily caused by dural thickening, permitting no reliable identification of bifurcations or other prominent vascular structures. In all other cases, one to four vascular anatomic points were identified and the Euclidean distance to the corresponding preMRI data calculated (**Figure 1**). For each case the mean Euclidean distance of the marked points was calculated, ranging from 2.6 to 6.0 mm (mean \pm SD = 4.1 ± 1.3 mm). Post-resectionally, 3D iUS Doppler was conducted in all six cases. Here, we found a Euclidean distance of 4.7 ± 1.0 mm (mean \pm SD), ranging from 2.9 to 6.0 mm. All measurements are shown in **Table 2**. Interestingly, apart from one measured value in case no. 2, the measured Euclidean distances within each case did not vary much, suggesting that the mean value can give a good indication for the estimation of the local brain deformation. Interestingly, according to our measurements the extent of pre-resectional and post-resectional shift of vascular landmarks is similar (mean of differences: 0.55 mm), without statistically significant differences ($p = 0.625$; paired t-test), as shown in an illustrative example in **Figure 2**. This is in contrast to the generally accepted assumption that the main shifting occurs after durotomy, as shown by Hill et al., who found a dural displacement of only 1.2 ± 2.0 mm (mean \pm SD) after craniotomy, but a brain shift of 4.4 ± 1.9 mm (immediately after dural opening) and of 5.6 ± 1.9 mm (approximately 1 h later), respectively (29). On the other hand, Ohue et al. described a displacement of tumor margins of 3.4 ± 1.9 mm (mean \pm SD) after craniotomy but before durotomy, which increased to 5.1 ± 2.7 mm, when the dura mater was opened (22). Similar findings were reported by Lettboer et al., who found the main displacement after craniotomy but reported an additional

shift of only 0.2 mm once the dural layer was opened (52). Regarding the pre-durotomy shift, our results are well in line with those of Ohue et al. and Lettboer et al., but one would expect more additional brain deformation after tumor resection as demonstrated, for example, by Roberts et al., who found a mean displacement of 1 cm (24). Yet there is a high variability in the extent of brain shift (25), and particularly deeper located structures are less prone to shifting (25, 53), which could also apply for the vascular structures and thus explain our results. Sastry et al. attributed the observation of a rather small post-durotomy shift to registration errors (38). In an earlier study, we determined the accuracy of the co-registration of the precalibrated ultrasound probe, using a tracked ultrasound phantom containing wires, and found an offset of 1.33 ± 0.33 (mean \pm SD) (50). Given this and the here calculated high registration accuracy, we consider the influence of the registration inaccuracies to be minor on our results. Care has to be taken when interpreting our results of the rather small brain shift of deeper located vessels in this study, as in many surgical situations already a little spatial offset of vascular structures could have devastating effects, if not considered by the surgeon. With that in mind, Šteňo et al. described the visualization of lenticulostriate arteries during the resection of insular low-grade gliomas using navigated 3D power Doppler and found this to be a promising approach to increase safety during the surgical course (54).

During surgery the main region of interest with respect to brain shift is the tumor surrounding area, and the actual brain deformation present there might be underestimated by measuring the movement of distant vascular landmarks. In our study, i3D US color Doppler did not depict small peritumoral vessels with such a high resolution that allowed analysis of shifting when compared to preMRI. Regarding this, a reasonable alternative to color Doppler is power Doppler, which does not measure the velocity and direction of the Doppler signal (and thus blood flow) but the power (amplitude) of the signal (55). Power Doppler allows detection of smaller vessels with less blood flow (55, 56), such as peritumoral vascular structures, and is less prone to typical color Doppler limitations and artifacts, like angle dependency or aliasing. Color Doppler is angle dependent, because it depicts the velocity along the ultrasound beam direction and not the true blood flow velocity, and thus, it is not able to detect flow perpendicular to the ultrasound beam. Aliasing occurs when the pulse rate limitation of the ultrasound transducer is exceeded or with inadequate velocity scale settings, resulting in incorrect pixel values. Neither applies for power Doppler, because it is not based on velocity measurements (55, 57). Additionally, power Doppler has less noise artifacts, which can be influenced by Doppler gain settings (38, 57). On the other hand, the power Doppler signal has a tendency to extend beyond the borders of vessels, which consequently appear thicker than they actually are, and the visualization of too many surgically not important vessels might result in rather confusing imaging (58).

Recently, contrast-enhanced ultrasound (CEUS) has been introduced as a real-time imaging in neurosurgical procedures, facilitating identification of pathological tissue and tumor blood

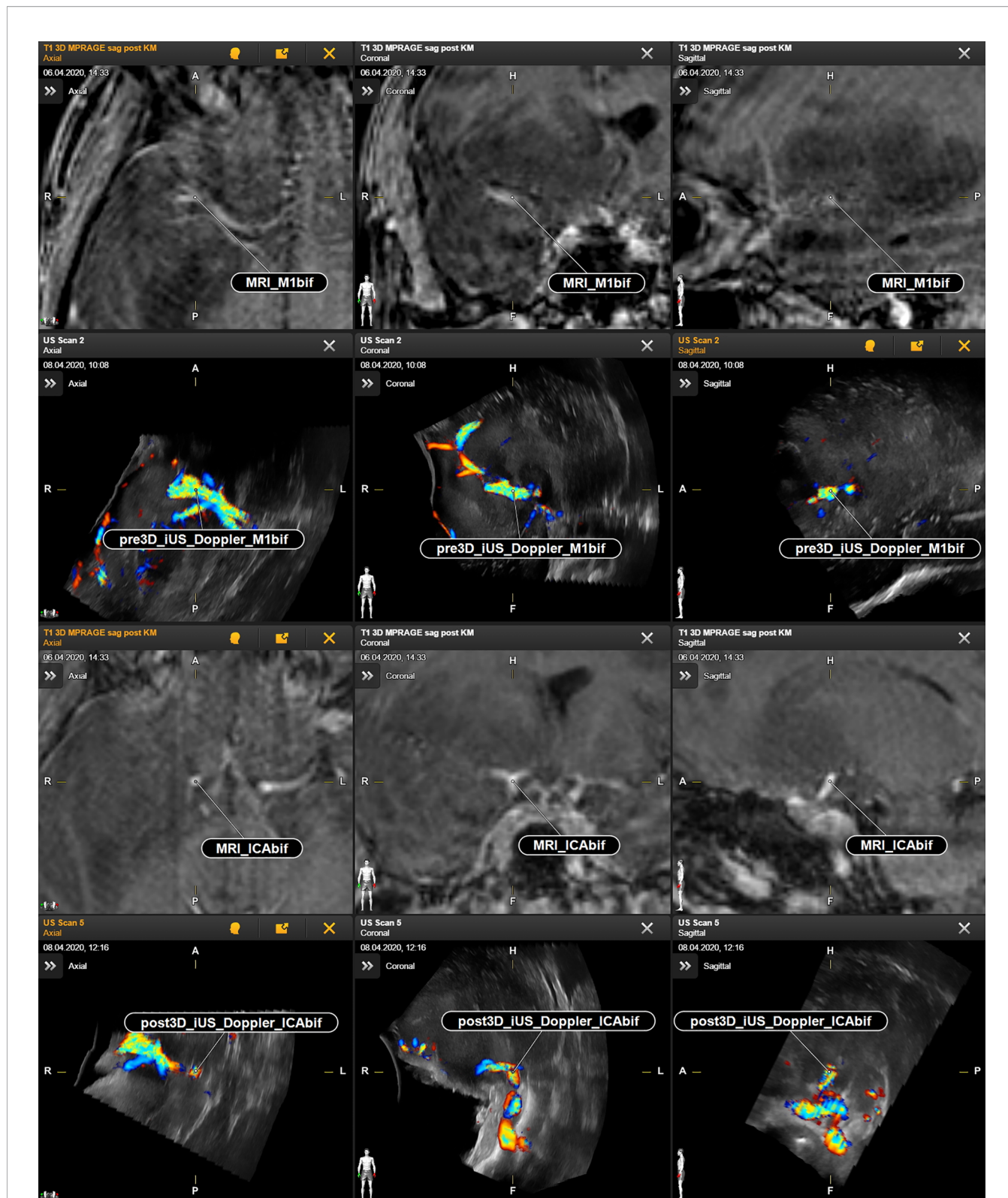


FIGURE 1 | Case no. 2. Identification of vascular anatomic landmarks in MRI and navigated reformatted 3D iUS Doppler. First and second row: preoperative MRI and corresponding pre-resectional 3D iUS Doppler in axial, coronal, and sagittal plane. Third and fourth row: preoperative MRI and corresponding post-resectional 3D iUS Doppler in axial, coronal, and sagittal plane. CAbif, internal carotid artery bifurcation; M1bif, M1bifurcation; pre3D iUS Doppler, pre-resectional 3D iUS Doppler; post3D iUS Doppler, post-resectional 3D iUS Doppler.

TABLE 2 | Measurements.

Case	pre3D iUS Doppler vs. preMRI			post3D iUS Doppler vs. preMRI		
	Vascular Structure	Euclidean Distance [mm]	Mean Euclidean Distance [mm]	Vascular Structure	Euclidean distance [mm]	Mean Euclidean Distance [mm]
1	ICAbif	5.1	6.0	ICAbif	4.9	5.0
	M1bif	6.9		M1bif	5.0	
2	ICAbif	3.8	3.5	ICAbif	2.4	2.9
	M1bif	3.4		M1bif	3.4	
	M2bif	4.9		M2bif	3.0	
	M1cont	1.86		M1cont	2.9	
3	–	–	–	ACIbif	5.2	5.2
				Basilar tip	5.1	
4	ICAbif	4.5	4.3	ICAbif	3.4	4.5
	M1bif	4.0		M1bif	5.5	
5	–	–	4.0	ICAbif	6.2	6.0
				M1bif	5.7	
6	ICAbif	3.2	2.6	ICAbif	6.2	4.8
	M1bif	2.0		Basilar tip	4.1	
				A2	4.2	

A2, A2 segment of anterior cerebral artery; ICAbif, internal carotid artery bifurcation; M1bif, M1 bifurcation segment of the MCA; M1cont, vascular contact of M1 to another vascular branch; M2, M2 segment of MCA; MCA, middle cerebral artery; pre3D iUS Doppler, pre-resectional 3D iUS Doppler; post3D iUS Doppler, post-resectional 3D iUS Doppler.

supply (59). Ilunga-Mbuyamba et al. acquired intraoperative CEUS and compared it to preoperative MRI data, using an algorithm for image registration. They described a good delineation of smaller vessels and used those data to estimate brain shift (60).

Our study was partially limited by the quality of the 3D iUS Doppler datasets, hampering the identification of landmarks. Additionally, we were confronted with several problems when segmenting the vascular tree. Preoperative MRI segmentation of the vessels was performed automatically in TOF or T1 contrast-enhanced sequences, or, alternatively, using the computer-assisted segmentation *via* the smart brush tool, depending on the quality of the auto-segmented objects. However, in 3D iUS Doppler ultrasound, neither automatic segmentation nor generation of objects using simple thresholding is currently available in the navigational software. Therefore, the vascular tree had to be manually segmented with the smart brush tool, which turned out to be a challenging and time-consuming procedure due to

artifacts in the reconstructed and reformatted datasets. Whilst a rough segmentation and identification of vascular landmarks could be performed during surgery by either a neurosurgeon or a trained computer scientist experienced in this field within 5–10 minutes, thorough segmentation using the smart brush tool was more complex and not feasible during the surgical procedure at this stage. Segmentation of small perivascular vessels in ultrasound datasets, which could have been localized with power Doppler or CEUS, using the smart brush tool, and manual identification of corresponding landmarks (e.g., vascular bifurcation) in the peritumoral region would have prolonged the whole procedure dramatically, if even possible. Thus, we focused on greater vascular structures, which could be identified in color Doppler and did not include power Doppler or CEUS analysis. Nevertheless, given a future implementation of automatic ultrasound segmentation into the navigational software, both share a great potential in the field of local brain shift estimation by delineating small peritumoral vessels.

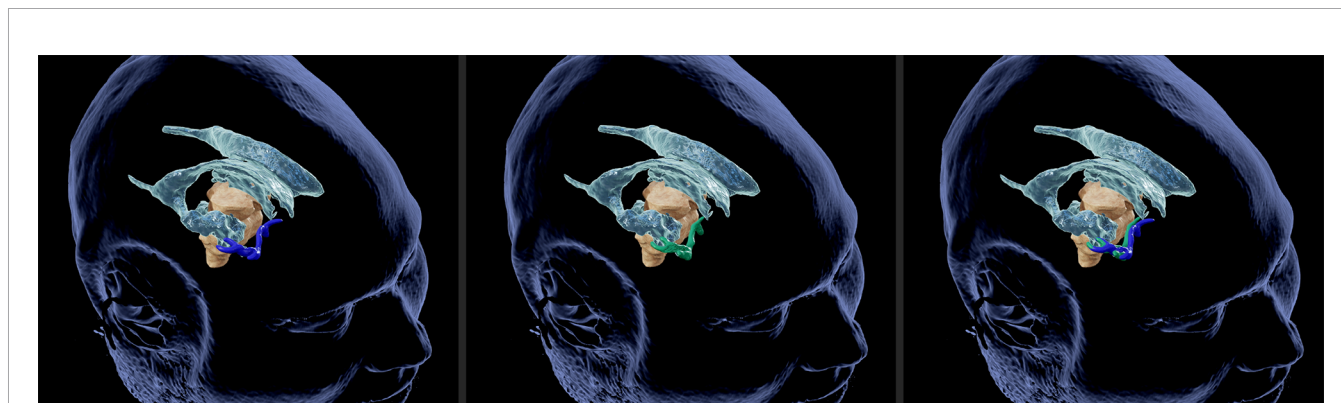


FIGURE 2 | Illustrative case no. 2. 3D view of vascular landmarks segmented in MRI (left) and US (middle). Combined presentation of both segmentations (right) depicts the spatial overlap.

Another option would have been to utilize third-party applications for the analysis of the vessel tree and to transfer the data back to the navigational system. This would allow deeper exploration of approaches, as the one proposed by Reinertsen et al., who used vascular centerlines for the calculation of brain deformation (37, 46). However, here we focused on the built-in features of the navigational system to test for intraoperative applicability. To increase usability and efficiency, the analysis tools should be implemented into the navigational software itself, e.g., for automatic identification and correction of brain shift after 3D iUS Doppler acquisition.

This work involved only patients with temporal mass lesions. We chose this approach to allow good visualization of the vascular tree encompassing, if available, the internal carotid artery, the A1/A2 segment of the anterior cerebral artery, and the M1/M2 segment of the medial cerebral artery, and to make our result more comparable to each other. On the other hand, this patient inclusion criterion makes it difficult to generalize the study results to differently located tumors, in which visualization of the vascular tree may be less successful. Eventually, this study cannot describe the impact of 3D iUS Doppler on every kind of brain tumor resection, but only for those cases in which the deeply located vascular structures are easily depictable in Doppler imaging. Finally, due to the limited number of identified corresponding anatomical landmarks, the here described approach does not allow full correction of brain shift within the navigational system yet. Identification of more representative landmarks or vascular segments would allow fusion of preoperative and intraoperative imaging as shown by Rasmussen et al., who have found satisfactory results in five cases of automatic multimodal fusion of preMRI and i3D US Doppler postoperatively and proposed intraoperative use of their technique (45).

Despite these limitations, we found 3D iUS Doppler to be a valuable adjunct to our multimodal navigational setup. In the current setup, identification of vascular landmarks in color Doppler imaging allows intraoperatively estimation of local brain shift and thus increases safety during resection. Future

implementation of automatic segmentation in ultrasound imaging or the possibility of generating objects *via* simple thresholding would facilitate further analysis of the vascular anatomy and brain shift and might allow navigational updating using 3D iUS Doppler datasets. Under these conditions, the advantages of power Doppler mode and CEUS could be fully exploited, and it will be of great interest to find out which type of vascular imaging contributes best and most feasibly to the determination of brain shift.

DATA AVAILABILITY STATEMENT

The original contributions presented in the study are included in the article/supplementary material. Further inquiries can be directed to the corresponding author.

ETHICS STATEMENT

The studies involving human participants were reviewed and approved by Ethikkommission der Philipps Universität Marburg, Fachbereich Medizin. The patients/participants provided their written informed consent to participate in this study.

AUTHOR CONTRIBUTIONS

Conceptualization, MB, CN, BS. Methodology, MB and BS. Validation, BC, CN, and MP. Investigation, MB, BS, and DZ. Resources, MB, BC, CN, MP, BS, and DZ. Data curation, MB and BS. Writing—original draft preparation, BS. Writing—review and editing, MB and CN. Visualization, MB and BS. Supervision, MB, CN, and BS. Project administration, MB. All authors contributed to the article and approved the submitted version.

REFERENCES

- Ostrom QT, Gittleman H, Fulop J, Liu M, Blanda R, Kromer C, et al. CBTRUS Statistical Report: Primary Brain and Central Nervous System Tumors Diagnosed in the United States in 2008–2012. *Neuro Oncol* (2015) 17(Suppl 4):iv1–62. doi: 10.1093/neuonc/nov189
- Sharma A, Graber JJ. Overview of Prognostic Factors in Adult Gliomas. *Ann Palliat Med* (2021) 10(1):863–74. doi: 10.21037/apm-20-640
- Claus EB, Walsh KM, Wiencke JK, Molinaro AM, Wiemels JL, Schildkraut JM, et al. Survival and Low-Grade Glioma: The Emergence of Genetic Information. *Neurosurg Focus* (2015) 38(1):E6. doi: 10.3171/2014.10.FOCUS12367
- Weller M, van den Bent M, Tonn JC, Stupp R, Preusser M, Cohen-Jonathan-Moyal E, et al. European Association for Neuro-Oncology (EANO) Guideline on the Diagnosis and Treatment of Adult Astrocytic and Oligodendroglial Gliomas. *Lancet Oncol* (2017) 18(6):e315–29. doi: 10.1016/S1470-2045(17)30194-8
- Pallud J, Varlet P, Devaux B, Geha S, Badoual M, Deroulers C, et al. Diffuse Low-Grade Oligodendrogliomas Extend Beyond MRI-Defined Abnormalities. *Neurology* (2010) 74(21):1724–31. doi: 10.1212/WNL.0b013e3181e04264
- Kelly PJ, Dumas-Duport C, Kispert DB, Kall BA, Scheithauer BW, Illig JJ. Imaging-Based Stereotaxic Serial Biopsies in Untreated Intracranial Glial Neoplasms. *J Neurosurg* (1987) 66(6):865–74. doi: 10.3171/jns.1987.66.6.0865
- Burger PC, Heinz ER, Shibata T, Kleihues P. Topographic Anatomy and CT Correlations in the Untreated Glioblastoma Multiforme. *J Neurosurg* (1988) 68(5):698–704. doi: 10.3171/jns.1988.68.5.0698
- Silbergeld DL, Chicoine MR. Isolation and Characterization of Human Malignant Glioma Cells From Histologically Normal Brain. *J Neurosurg* (1997) 86(3):525–31. doi: 10.3171/jns.1997.86.3.0525
- Brown TJ, Brennan MC, Li M, Church EW, Brandmeir NJ, Rakszawski KL, et al. Association of the Extent of Resection With Survival in Glioblastoma: A Systematic Review and Meta-Analysis. *JAMA Oncol* (2016) 2(11):1460–9. doi: 10.1001/jamaoncol.2016.1373
- Grabowski MM, Recinos PF, Nowacki AS, Schroeder JL, Angelov L, Barnett GH, et al. Residual Tumor Volume Versus Extent of Resection: Predictors of Survival After Surgery for Glioblastoma. *J Neurosurg* (2014) 121(5):1115–23. doi: 10.3171/2014.7.JNS132449

11. Kreth FW, Thon N, Simon M, Westphal M, Schackert G, Nikkha G, et al. Gross Total But Not Incomplete Resection of Glioblastoma Prolongs Survival in the Era of Radiochemotherapy. *Ann Oncol* (2013) 24(12):3117–23. doi: 10.1093/annonc/mdt388
12. Li YM, Suki D, Hess K, Sawaya R. The Influence of Maximum Safe Resection of Glioblastoma on Survival in 1229 Patients: Can We do Better Than Gross-Total Resection? *J Neurosurgery* (2016) 124(4):977–88. doi: 10.3171/2015.5.JNS142087
13. Almeida JP, Chaichana KL, Rincon-Torroella J, Quinones-Hinojosa A. The Value of Extent of Resection of Glioblastomas: Clinical Evidence and Current Approach. *Curr Neurol Neurosci Rep* (2015) 15(2):517. doi: 10.1007/s11910-014-0517-x
14. Bayer S, Maier A, Ostermeier M, Fahrig R. Intraoperative Imaging Modalities and Compensation for Brain Shift in Tumor Resection Surgery. *Int J BioMed Imaging* (2017) 2017:6028645. doi: 10.1155/2017/6028645
15. Uhl E, Zausinger S, Morhard D, Heigl T, Scheder B, Rachinger W, et al. Intraoperative Computed Tomography With Integrated Navigation System in a Multidisciplinary Operating Suite. *Neurosurgery* (2009) 64(5 Suppl 2):231–9discussion 9–40. doi: 10.1227/01.NEU.0000340785.51492.B5
16. Hosoda T, Takeuchi H, Hashimoto N, Kitai R, Arishima H, Kodera T, et al. Usefulness of Intraoperative Computed Tomography in Surgery for Low-Grade Gliomas: A Comparative Study Between Two Series Without and With Intraoperative Computed Tomography. *Neurol Med Chir (Tokyo)* (2011) 51(7):490–5. doi: 10.2176/nmc.51.490
17. Barbagallo GMV, Palmucci S, Visocchi M, Paratore S, Attina G, Sortino G, et al. Portable Intraoperative Computed Tomography Scan in Image-Guided Surgery for Brain High-Grade Gliomas: Analysis of Technical Feasibility and Impact on Extent of Tumor Resection. *Oper Neurosurg (Hagerstown)* (2016) 12(1):19–30. doi: 10.1227/NEU.0000000000001112
18. Senft C, Bink A, Franz K, Vatter H, Gasser T, Seifert V. Intraoperative MRI Guidance and Extent of Resection in Glioma Surgery: A Randomised, Controlled Trial. *Lancet Oncol* (2011) 12(11):997–1003. doi: 10.1016/S1470-2045(11)70196-6
19. Kuhnt D, Ganslandt O, Schlaffer SM, Buchfelder M, Nimsky C. Quantification of Glioma Removal by Intraoperative High-Field Magnetic Resonance Imaging: An Update. *Neurosurgery* (2011) 69(4):852–62discussion 62–3. doi: 10.1227/NEU.0b013e318225ea6b
20. Kuhnt D, Bauer MH, Nimsky C. Brain Shift Compensation and Neurosurgical Image Fusion Using Intraoperative MRI: Current Status and Future Challenges. *Crit Rev BioMed Eng* (2012) 40(3):175–85. doi: 10.1615/CritRevBiomedEng.v40.i3.20
21. Gerganov VM, Samii A, Giordano M, Samii M, Fahlbusch R. Two-Dimensional High-End Ultrasound Imaging Compared to Intraoperative MRI During Resection of Low-Grade Gliomas. *J Clin Neurosci* (2011) 18(5):669–73. doi: 10.1016/j.jocn.2010.08.017
22. Ohue S, Kumon Y, Nagato S, Kohno S, Harada H, Nakagawa K, et al. Evaluation of Intraoperative Brain Shift Using an Ultrasound-Linked Navigation System for Brain Tumor Surgery. *Neurol Med Chir (Tokyo)* (2010) 50(4):291–300. doi: 10.2176/nmc.50.291
23. Gronningsaeter A, Kleven A, Ommedal S, Aarseth TE, Lie T, Lindseth F, et al. SonoWand, an Ultrasound-Based Neuronavigation System. *Neurosurgery* (2000) 47(6):1373–9discussion 9–80. doi: 10.1093/neurosurgery/47.6.1373
24. Roberts DW, Hartov A, Kennedy FE, Miga MI, Paulsen KD. Intraoperative Brain Shift and Deformation: A Quantitative Analysis of Cortical Displacement in 28 Cases. *Neurosurgery* (1998) 43(4):749–58discussion 58–60. doi: 10.1097/00006123-199810000-00010
25. Nimsky C, Ganslandt O, Cerny S, Hastreiter P, Greiner G, Fahlbusch R. Quantification of, Visualization of, and Compensation for Brain Shift Using Intraoperative Magnetic Resonance Imaging. *Neurosurgery* (2000) 47(5):1070–9. doi: 10.1097/00006123-200011000-00008
26. Kelly PJ, Kall BA, Goerss S, Earnest FT. Computer-Assisted Stereotaxic Laser Resection of Intra-Axial Brain Neoplasms. *J Neurosurg* (1986) 64(3):427–39. doi: 10.3171/jns.1986.64.3.0427
27. MA Audette, K Siddiqi, TM Peters eds. *Level-Set Surface Segmentation and Fast Cortical Range Image Tracking for Computing Intrasurgical Deformations*. Berlin, Heidelberg: Springer Berlin Heidelberg (1999). doi: 10.1007/10704282_86
28. Dorward NL, Alberti O, Velani B, Gerritsen FA, Harkness WF, Kitchen ND, et al. Postimaging Brain Distortion: Magnitude, Correlates, and Impact on Neuronavigation. *J Neurosurg* (1998) 88(4):656–62. doi: 10.3171/jns.1998.88.4.0656
29. Hill DL, Maurer CR Jr., Maciunas RJ, Barwise JA, Fitzpatrick JM, Wang MY. Measurement of Intraoperative Brain Surface Deformation Under a Craniotomy. *Neurosurgery* (1998) 43(3):514–26. doi: 10.1097/00006123-199809000-00066
30. Wirtz CR, Bonsanto MM, Knauth M, Tronnier VM, Albert FK, Stauber A, et al. Intraoperative Magnetic Resonance Imaging to Update Interactive Navigation in Neurosurgery: Method and Preliminary Experience. *Comput Aided Surg* (1997) 2(3–4):172–9. doi: 10.3109/10929089709148110
31. Nimsky C, Ganslandt O, Hastreiter P, Fahlbusch R. Intraoperative Compensation for Brain Shift. *Surg Neurol* (2001) 56(6):357–64. doi: 10.1016/S0090-3019(01)00628-0
32. Buchholdz RD, Yeh DD, Trobaugh J, McDurmount LL, Sturm CD, Baumann C, et al eds. *The Correction of Stereotactic Inaccuracy Caused by Brain Shift Using an Intraoperative Ultrasound Device*. Berlin, Heidelberg: Springer Berlin Heidelberg (1997). 10.1007/BFb0029268
33. Jodicke A, Deinsberger W, Erbe H, Kriete A, Boker DK. Intraoperative Three-Dimensional Ultrasonography: An Approach to Register Brain Shift Using Multidimensional Image Processing. *Minim Invasive Neurosurg* (1998) 41(1):13–9. doi: 10.1055/s-2008-1052008
34. Comeau RM, Fenster A, Peters TM. Intraoperative US in Interactive Image-Guided Neurosurgery. *Radiographics* (1998) 18(4):1019–27. doi: 10.1148/radiographics.18.4.9672984
35. Nabavi A, Black PM, Gering DT, Westin CF, Mehta V, Pergolizzi RS Jr., et al. Serial Intraoperative Magnetic Resonance Imaging of Brain Shift. *Neurosurgery* (2001) 48(4):787–97discussion 97–8. doi: 10.1227/00006123-200104000-00019
36. Nimsky C, Ganslandt O, von Keller B, Romstock J, Fahlbusch R. Intraoperative High-Field-Strength MR Imaging: Implementation and Experience in 200 Patients. *Radiology* (2004) 233(1):67–78. doi: 10.1148/radiol.2331031352
37. Reinertsen I, Lindseth F, Askeland C, Iversen DH, Unsgard G. Intra-Operative Correction of Brain-Shift. *Acta Neurochir (Wien)* (2014) 156(7):1301–10. doi: 10.1007/s00701-014-2052-6
38. Sastry R, Bi WL, Pieper S, Frisken S, Kapur T, Wells W3rd, et al. Applications of Ultrasound in the Resection of Brain Tumors. *J Neuroimaging* (2017) 27(1):5–15. doi: 10.1111/jon.12382
39. Unsgaard G, Ommedal S, Muller T, Gronningsaeter A, Nagelhus Hernes TA. Neuronavigation by Intraoperative Three-Dimensional Ultrasound: Initial Experience During Brain Tumor Resection. *Neurosurgery* (2002) 50(4):804–12discussion 12. doi: 10.1097/00006123-200204000-00022
40. Tronnier VM, Bonsanto MM, Stauber A, Knauth M, Kunze S, Wirtz CR. Comparison of Intraoperative MR Imaging and 3D-Navigated Ultrasonography in the Detection and Resection Control of Lesions. *Neurosurg Focus* (2001) 10(2):E3. doi: 10.3171/foc.2001.10.2.4
41. Munkvold BKR, Jakola AS, Reinertsen I, Sagberg LM, Unsgard G, Solheim O. The Diagnostic Properties of Intraoperative Ultrasound in Glioma Surgery and Factors Associated With Gross Total Tumor Resection. *World Neurosurg* (2018) 115:e129–e36. doi: 10.1016/j.wneu.2018.03.208
42. Keles GE, Lamborn KR, Berger MS. Coregistration Accuracy and Detection of Brain Shift Using Intraoperative Sononavigation During Resection of Hemispheric Tumors. *Neurosurgery* (2003) 53(3):556–62discussion 62–4. doi: 10.1227/01.NEU.0000080949.44837.AC
43. Pallatroni H, Hartov A, McInerney J, Platenik LA, Miga MI, Kennedy FE, et al. Coregistered Ultrasound as a Neurosurgical Guide. *Stereot Funct Neuros* (1999) 73(1–4):143–7. doi: 10.1159/000029775
44. Slomka PJ, Mandel J, Downey D, Fenster A. Evaluation of Voxel-Based Registration of 3-D Power Doppler Ultrasound and 3-D Magnetic Resonance Angiographic Images of Carotid Arteries. *Ultrasound Med Biol* (2001) 27(7):945–55. doi: 10.1016/S0301-5629(01)00387-8
45. Rasmussen IA Jr., Lindseth F, Rygh OM, Berntsen EM, Selbekk T, Xu J, et al. Functional Neuronavigation Combined With Intra-Operative 3D Ultrasound: Initial Experiences During Surgical Resections Close to Eloquent Brain Areas and Future Directions in Automatic Brain Shift Compensation of Preoperative Data. *Acta Neurochir (Wien)* (2007) 149(4):365–78. doi: 10.1007/s00701-006-1110-0
46. Reinertsen I, Lindseth F, Unsgaard G, Collins DL. Clinical Validation of Vessel-Based Registration for Correction of Brain-Shift. *Med Image Anal* (2007) 11(6):673–84. doi: 10.1016/j.media.2007.06.008

47. Podlesek D, Meyer T, Morgenstern U, Schackert G, Kirsch M. Improved Visualization of Intracranial Vessels With Intraoperative Coregistration of Rotational Digital Subtraction Angiography and Intraoperative 3D Ultrasound. *PLoS One* (2015) 10(3):e0121345. doi: 10.1371/journal.pone.0121345
48. Mohammadi A, Ahmadian A, Azar AD, Sheykh AD, Amiri F, Alirezaie J. Estimation of Intraoperative Brain Shift by Combination of Stereovision and Doppler Ultrasound: Phantom and Animal Model Study. *Int J Comput Assist Radiol Surg* (2015) 10(11):1753–64. doi: 10.1007/s11548-015-1216-z
49. Mohammadi A, Ahmadian A, Rabbani S, Fattahi E, Shirani S. A Combined Registration and Finite Element Analysis Method for Fast Estimation of Intraoperative Brain Shift; Phantom and Animal Model Study. *Int J Med Robot* (2017) 13(4):1–8. doi: 10.1002/rcs.1792
50. Saß B, Carl B, Pojskic M, Nimsky C, Bopp M. Navigated 3d Ultrasound in Brain Metastasis Surgery: Analyzing the Differences in Object Appearances in Ultrasound and Magnetic Resonance Imaging. *Appl Sci* (2020) 10(21):7798. doi: 10.3390/app10217798
51. Carl B, Bopp M, Sass B, Nimsky C. Intraoperative Computed Tomography as Reliable Navigation Registration Device in 200 Cranial Procedures. *Acta Neurochir (Wien)* (2018) 160(9):1681–9. doi: 10.1007/s00701-018-3641-6
52. Letteboer MM, Willems PW, Viergever MA, Niessen WJ. Brain Shift Estimation in Image-Guided Neurosurgery Using 3-D Ultrasound. *IEEE Trans BioMed Eng* (2005) 52(2):268–76. doi: 10.1109/TBME.2004.840186
53. Ganser KA, Dickhaus H, Staubert A, Bonsanto MM, Wirtz CR, Tronnier VM, et al. Quantification of Brain Shift Effects in MRI Images. *BioMed Tech (Berl)* (1997) 42 Suppl:247–8. doi: 10.1515/bmte.1997.42.s2.247
54. Steno A, Jezberova M, Holly V, Timarova G, Steno J. Visualization of Lenticulostriate Arteries During Insular Low-Grade Glioma Surgeries by Navigated 3D Ultrasound Power Doppler: Technical Note. *J Neurosurg* (2016) 125(4):1016–23. doi: 10.3171/2015.10.JNS151907
55. Anderson T, McDicken WN. The Difference Between Colour Doppler Velocity Imaging and Power Doppler Imaging. *Eur J Echocardiogr* (2002) 3(3):240–4. doi: 10.1053/euje.3.3.240
56. Martinoli C, Pretolesi F, Crespi G, Bianchi S, Gandolfo N, Valle M, et al. Power Doppler Sonography: Clinical Applications. *Eur J Radiol* (1998) 27 Suppl 2:S133–40. doi: 10.1016/S0720-048X(98)00054-0
57. Pozniak MA, Zagzebski JA, Scanlan KA. Spectral and Color Doppler Artifacts. *Radiographics* (1992) 12(1):35–44. doi: 10.1148/radiographics.12.1.1734480
58. Rygh OM, Nagelhus Hernes TA, Lindseth F, Selbekk T, Brostrup Muller T, Unsgaard G. Intraoperative Navigated 3-Dimensional Ultrasound Angiography in Tumor Surgery. *Surg Neurol* (2006) 66(6):581–92: discussion 92. doi: 10.1016/j.surneu.2006.05.060
59. Prada F, Del Bene M, Mattei L, Lodigiani L, DeBeni S, Kolev V, et al. Preoperative Magnetic Resonance and Intraoperative Ultrasound Fusion Imaging for Real-Time Neuronavigation in Brain Tumor Surgery. *Ultraschall Med* (2015) 36(2):174–86. doi: 10.1055/s-0034-1385347
60. Ilunga-Mbuyamba E, Avina-Cervantes JG, Lindner D, Cruz-Aceves I, Arlt F, Chalopin C. Vascular Structure Identification in Intraoperative 3d Contrast-Enhanced Ultrasound Data. *Sensors (Basel)* (2016) 16(4):1–14. doi: 10.3390/s16040497

Conflict of Interest: CN and MB are consultants for Brainlab.

The remaining authors declare that the research was conducted in the absence of any commercial or financial relationships that could be construed as a potential conflict of interest.

Publisher's Note: All claims expressed in this article are solely those of the authors and do not necessarily represent those of their affiliated organizations, or those of the publisher, the editors and the reviewers. Any product that may be evaluated in this article, or claim that may be made by its manufacturer, is not guaranteed or endorsed by the publisher.

Copyright © 2021 Saß, Pojskic, Zivkovic, Carl, Nimsky and Bopp. This is an open-access article distributed under the terms of the Creative Commons Attribution License (CC BY). The use, distribution or reproduction in other forums is permitted, provided the original author(s) and the copyright owner(s) are credited and that the original publication in this journal is cited, in accordance with accepted academic practice. No use, distribution or reproduction is permitted which does not comply with these terms.